CHIN. PHYS. LETT. Vol. 35, No. 9 (2018) 097102

Electronic Phase Transition of $IrTe_2$ Probed by Second Harmonic Generation *

J. E. Taylor[1], Z. Zhang[1], G. Cao[1], L. H. Haber[2], R. Jin[1], E. W. Plummer[1]**

[1]*Department of Physics & Astronomy, Louisiana State University, LA 70803, USA*
[2]*Department of Chemistry, Louisiana State University, LA 70803, USA*

(Received 28 August 2018)

We have utilized second harmonic generation (SHG) to disentangle the coupled first-order charge order/structural transition at $T_c \sim 281\,K$ in the transition-metal dichalocogenide $IrTe_2$, an exceptional layered material with 3D properties. The data from SHG shows extremely sharp transition in both the cooling and warming processes with less than 0.2 K transition window. Surface electronic symmetries of C_{3v} and S_2 are observed in the high temperature and low temperature phases, respectively. Compared to neutron diffraction data for the structural transition (Phys. Rev. B 88 (2013) 115122) and to the electrical resistivity for the microscopic transition (Phys. Rev. B 95 (2017) 035148), our data indicates the electronic transition at the surface is the precursor to the structural transition.

PACS: 71.30.+h, 73.20.−r, 71.20.Be, 78.68.+m, 71.45.Lr DOI: 10.1088/0256-307X/35/9/097102

Transition-metal dichalocogenides (TMDs) have fascinated the community since the 1970s, one reason being the observation of pervasive charge density waves (CDWs),[1,2] and another being the display of exciting properties such as superconductivity[3–5] and topological behavior.[6] These materials with layered structures are easily exfoliated creating an opportunity for the development of two-dimensional devices.[7–9] $IrTe_2$ is a special TMD due to the unusual complexity, and the mystery surrounding the charge order/structural transition occurring at $T_c \sim 281\,K$. When $IrTe_2$ is in the high temperature phase ($T > T_c$), the compound's hexagonal lattice structure consists of edge-shared $IrTe_6$ octahedra forming the unit cell defined as $[1 \times 1 \times 1]$[10] with the first two indices in-plane (Fig. 1(a)). These octahedral slabs stack along the c axis creating a layered structure with $P\bar{3}m1$ (D^5_{3d}) symmetry. While TMDs commonly have their layers connected via weak van der Waals bonds, $IrTe_2$ exhibits shorter interlayer Te–Te distances compared to in-plane bond lengths.[11] This strange interlayer bonding is supported by band structure calculations of the high temperatures, where both bands and Fermi surface show three-dimensional character.[10,12] When cooled below T_c, $IrTe_2$ undergoes a first-order charge order/structural transition characterized by long-range reorganization in 3D resulting in a new structure shown in Fig. 1(b) with a unit cell defined by $[5 \times 1 \times 5]$.[10] The low temperature phase has a new triclinic $P\bar{1}$ symmetry (Fig. 1(b)). In this phase, the low temperature c' axis is no longer parallel with the original c axis at $T > T_c$.[12] Figure 1(c) shows the neutron diffraction measured structural transition as a function of temperature for using an integer diffraction peak.[10]

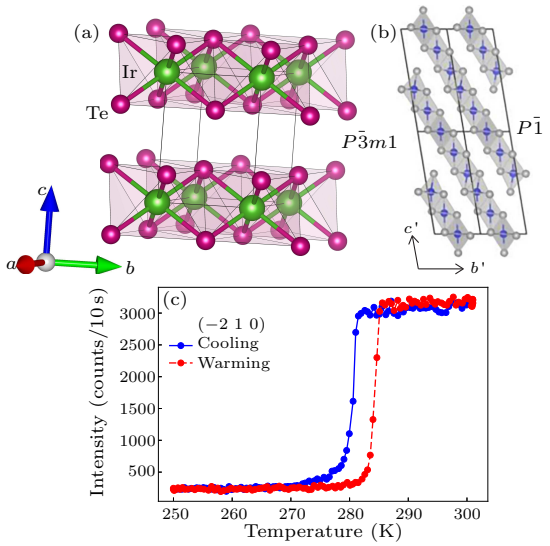

Fig. 1. (a) $IrTe_2$ trigonal unit cell. Green and pink balls correspond to Ir and Te atoms consisting of $IrTe_6$ octahedral building blocks. (b) $IrTe_2$ triclinic unit cell. Image from Ref. [11]. (c) Temperature dependence of the (−2 1 0) peak intensity measured by neutron diffraction:[10] blue circles represent cooling while red circles are for warming process.

As with most of the other TMDs, one of the first explanations of the transition was a Peierls instability[13,14] inducing a CDW; however, the lack of an observable CDW gap[15] or Fermi surface nesting has eliminated this simple model. Many other models have been proposed including anionic depolymerization of Te bonds,[16] instability in the Te 5p states at the Fermi energy,[10] Te 5p and Ir 5d orbital interaction,[17] orbital splitting of the Te 5p states,[15] and Ir–Ir dimerization.[12,18,19] Most significant for

*Supported by the National Science Foundation under Grant No DMR-1504226.
**Corresponding author. Email: wplummer@phys.lsu.edu
© 2018 Chinese Physical Society and IOP Publishing Ltd

$IrTe_2$ is the fact that the charge order/structural transition is three-dimensional. First principle calculations illustrate two apparently different explanations for the coupled transition in $IrTe_2$.[10,12] Both calculations used the generalized gradient approximation of Perdew, Burke and Ernzerhof (PBE)[20] and produced very similar density of states (DOS) near the Fermi energy for the high and low temperature phases. There are very general and important conclusions from these calculations: (1) The bands near the Fermi energy and the Fermi contours show dispersion in all directions. Electronically, this is not a layered material,[10,12] consistent with measured bond lengths.[11] (2) The Te and Ir bands are strongly hybridized, so it is impossible to separate Te and Ir bands, therefore nominal ionic models, e.g., $Ir^{4+}Te_2^{2-}$ (Refs. [1-9,11-21]) are not applicable. (3) The inclusion of dynamical mean field theory is not important for this system,[12] meaning this is not a localized or correlated system. What is important to this study is that one of the two first-principle calculations concludes that the transition results from an instability in the Te $5p$ states[10] and the other that the origin is the Ir–Ir dimerization.[12] Experimentally X-ray crystal structure refinement[12] shows Ir–Ir dimerization in the low temperature phase but cannot determine if the dimerization is the origin of the consequence of the transition.

To probe the nature of this transition we utilize second harmonic generation (SHG) to isolate the electronic transition. By comparing the temperature dependence of the SHG signal to the measured bulk structural (neutron scattering[10]) and electrical resistivity,[11] we can unravel the coupling of the electronic and structural transitions. SHG is a second-order nonlinear optical technique proven capable of probing electronic phases, even if the electronic phase is dissimilar to the structure phase.[21] A beautiful example is the use of SHG to identify a nematic phase in $Cd_2Re_2O_7$,[22] occurring when the symmetry of the charge is not the same as the lattice.[21] The sensitivity of SHG to the electronic symmetry lies in the induced second order polarization P_i, which can be expressed as

$$P_i(2\omega) = \chi^{(2)}_{ijk} E_j E_k, \tag{1}$$

where the second order susceptibility tensor $\chi^{(2)}_{ijk}$ represents the electronic response (charge) to two incident photons $E_j E_k$.[23] When the symmetry of the charge is centrosymmetric, $\chi^{(2)}_{ijk}$ is zero in the bulk, isolating the generation of second harmonic photons to surfaces where centrosymmetry is broken,[24] allowing SHG to directly probe electronic symmetry of material surfaces.

The rotational second harmonic generation optical setup is shown in Fig. 2. An amplified Ti:sapphire laser generates a 1 kHz pulse train of 100 fs pulses each centered at 800 nm (1.55 eV) with corresponding pulse energy of 3.6 mJ. Incident field polarization is selected via half-wave plate ($\lambda/2$) then focused onto a flat shiny spot on sample and collected using a collimating lens. The beam was focused to a ~120 micrometer spot size at an incident angle of 35° with a fluence of ~5 mJ/cm^2. Laser fluence was controlled using a neutral density filter. After a polarizer, the generated 400 nm (3.1 eV) photons were separated from the fundamental 800 nm photons using a low-pass filter, focused onto a monochromator, and collected via high-sensitivity charge-coupled device. Spectra and background are differentiated using a beam block prior to the sample. For rotational-SHG studies a piezo-driven rotational stage was used to azimuthally rotate $IrTe_2$ about the surface normal (001). The sample temperature was controlled by mounting the single crystal on top of a thermoelectric cooler under vacuum (10^{-3} Torr) and measured using a thermocouple attached to the sample (±0.2 K). Prior to temperature measurements, the sample was rotated to maximize the second harmonic intensity. It should be pointed out that using femtosecond pulses for SHG ensures that the lattice does not have time to respond to the excited electronic configuration.[25] High-quality $IrTe_2$ single crystals were grown using the self-flux method described in Ref. [11]. Single crystals were cleaved along the (110) plane in air using scotch tape.

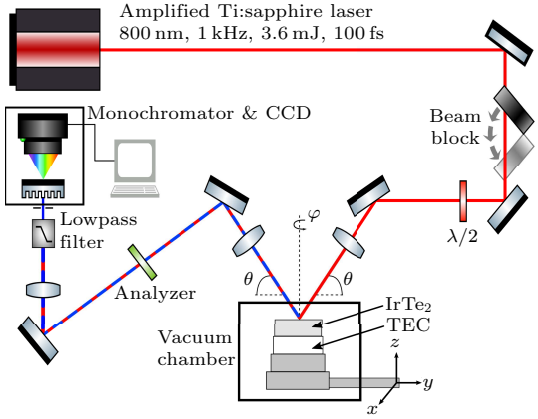

Fig. 2. Rotational second harmonic generation optical setup: 800 nm pulses are generated by an amplified Ti:sapphire laser and focused onto the $IrTe_2$ sample at $\Theta = 35°$. Temperature is controlled via thermoelectric cooler. The reflected 400 nm photons are filtered from the fundamental beam and focused onto a monochromator then collected using a charge-coupled device.

The measured azimuthal angle dependence, φ, of the second harmonic intensity at room temperature is shown in Figs. 3(a) and 3(b). From the data (green data points), P_{input}–P_{output} (PP) and S_{input}–S_{output} (SS) rotational-SHG plots exhibit a three-fold and six-fold angular dependence, respectively. PP is charac-

terized by three large intensity lobes spaced at 120° intervals with small intensity lobes in between. SS, on the other hand, has six equal intensity lobes spaced at 60° intervals. The measured intensity of the reflected second harmonic signal can be derived from the induced electric dipole (charge) as $I_{\rm SHG} = P^2(2\omega)$. In general for centrosymmetric materials, application of the space group symmetry to $\chi^{(2)}_{ijk}$ simplifies the second order susceptibility tensor. For a crystal of bulk space group D^5_{3d} the surface symmetry reduces to C_{3v} resulting in 27-element $\chi^{(2)}_{ijk}$ tensor consisting of only 4 non-vanishing elements: $\chi_{xxx} = -\chi_{xyy} = -\chi_{\rm yxy}, \chi_{zxx} = \chi_{zyy}, \chi_{xxz} = \chi_{yyz}$, and χ_{zzz}. More details regarding the derivation of these fit equations can be found in Ref. [26]. For PP and SS geometries, the reduced form of the second harmonic intensity are as follows:

$$I_{\rm PP} = A|a^{(2)} - a^{(1)}\cos(3\varphi)|^2, \quad (2)$$

$$I_{\rm SS} = A|a^{(1)}\sin(3\varphi)|^2, \quad (3)$$

where A is a geometric constant, $a^{(1)} \propto \chi_{xxx}$, and $a^{(2)} \propto \chi_{zzz} + \chi_{xxz} + \chi_{zxx}$.[27]

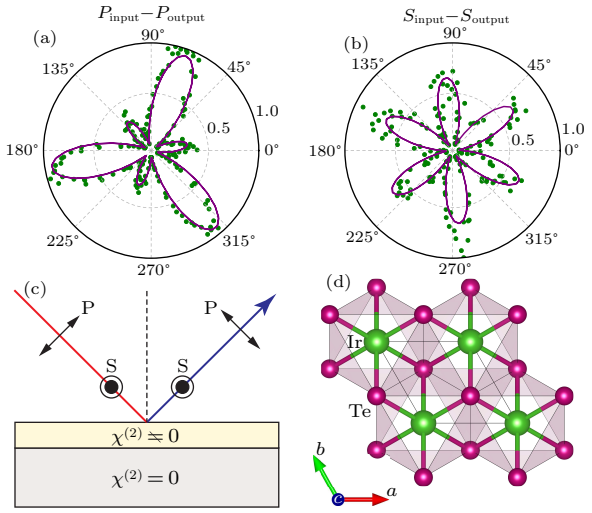

Fig. 3. Rotational-SHG polar plots for $P_{\rm input}$–$P_{\rm output}$ (a) and $S_{\rm input}$–$S_{\rm output}$ (b) combinations taken at room temperature. Green dots represent the data and purple lines are the theoretical fits to $I_{\rm PP}$ (Eq. (2)) and $I_{\rm SS}$ (Eq. (3)). (c) Second harmonic generation geometry. Out-of-plane polarization is defined as P and in-plane polarization is defined as S. (d) $IrTe_2$ C_{3v} surface.

Based on the polarization geometry in Fig. 3(c), S-polarized electric fields can only excite in-plane electronic states making $a^{(1)}$ sensitive to the in-plane electronic response. Conversely, P-polarized photons can only excite out-of-plane electronic states and therefore $a^{(2)}$ probes the out-of-plane electronic response. By comparing the polar fits to the C_{3v} crystal surface in Fig. 3(d), it is evident that the in-plane and out-of-plane responses originate from electrons with the symmetry of the high temperature phase. From the fit, we can conclude that the rotational-SHG measurements are in agreement with expected C_{3v} symmetry of the surface of $IrTe_2$.

The temperature evolution of the phase transition was obtained for both the PP and SS geometries. Figure 4(a) shows that, during the cooling process, there is a sharp decrease in the SHG intensity at $T_{\rm c,cooling} \sim 281$ K, as a result of the change in the symmetry of electronic states in the low temperature phase. Upon heating, a hysteric behavior in the second harmonic intensity is observed with $T_{\rm c,heating} \sim 283$ K, where the SHG intensity returns to its initial value. The measurement was repeated for the SS geometry and produced identical behavior, which in both cases is reversible and repeatable. The difference in the temperatures between the heating and cooling transitions is ~2 K, which is labeled ΔT. The transition for both cooling and heating processes occurs within <0.2 K, limited by the temperature steps.

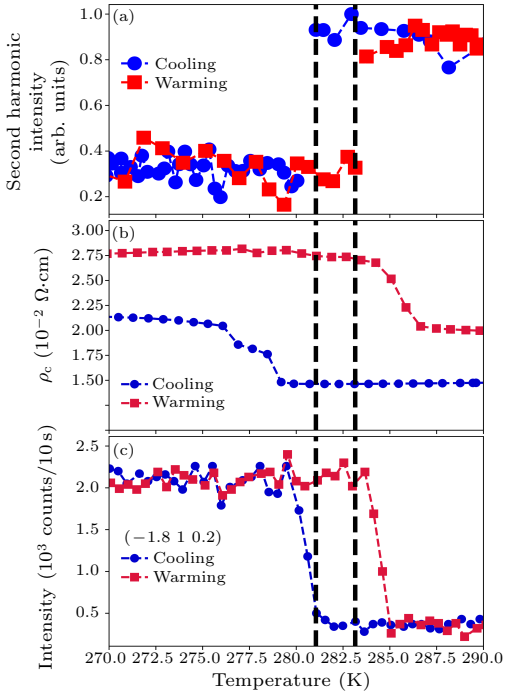

Fig. 4. (a) $P_{\rm input}$–$P_{\rm output}$ temperature dependence of the second harmonic intensity near $T_{\rm c}$. (b) Out-of-plane electronic resistivity.[11] (c) (−1.8 1 0.2) structural modulation observed by neutron diffraction.[10] Vertical lines mark the onset of the transition as seen by SHG.

The change in the SHG signal in Fig. 4(a) can be attributed to the first-order transition from C_{3v} to the new symmetry of the low temperature phase, which is S_2 (representing the $P\bar{1}$ space group). But in principle, the triclinic class has two possible space groups $P\bar{1}$ and $P1$ and both have been reported for $IrTe_2$.[4,11] The $P1$ space group is noncentrosymmetric, typically resulting in significantly larger second harmonic intensities, which is not what is observed. Most significant is the fact that the S_2 symmetry has no contribution for $\chi^{(2)}_{ijk}$, i.e. no SHG signal.[23] Therefore, the

low temperature phase belongs to the $P\bar{1}$ space group, in agreement with X-ray diffraction measurements.[11] The background second harmonic intensity seen in Fig. 4(a) is likely caused by surface imperfections and disorder resulting from the phase transition.[28,29] After completing the temperature cycle, the C_{3v} electronic symmetry is recoverable at room temperature.

In Figs. 4(b) and 4(c) we compare the measured transition from SHG to corresponding bulk measurements. Figure 4(b) shows the out-of-plane electrical resistivity from the same batch of single crystals used for SHG measurements.[11] From the electrical resistivity data, the observed ΔT of the hysteresis is $\sim$2 K while it takes $\sim$4 K for the transition to be completed. Neutron scattering probing the 3D transition associated with fractional order diffraction spots (−1.8 1 0.2) is shown in Fig. 4(c), with a $\Delta T \sim 2$ K and 1–2 K to complete the transition. For all three measurements, the ΔT of the hysteresis ($\sim$2 K) is more or less the same. The fact that the electronic (Fig. 4(a)) and structural transitions (Fig. 4(c)) have exactly the same hysteresis and T_c in heating and cooling show that both transitions are concomitant and subtle structural differences between surface and bulk[30] are not critical to electronic properties. However, the second harmonic intensity completes its transition between the high temperature phase and low temperature phase in <0.2 K, 4 times shorter than the structural transition, with even more significant difference from the bulk resistivity, indicating the surface electronic transition is much sharper than the bulk (in both heating and cooling).

In summary, second harmonic generation has been used to probe the temperature dependence of the electronic component of the charge ordered/structural transition in high-quality $IrTe_2$ single crystals. The electronic transition from a C_{3v} to S_2 symmetry is characterized by an abrupt change in intensity when crossing the transition, both in warming and cooling, limited by our instrumental set up. In contrast, the temperature range associated with the structural transition seen with neutron scattering is >4 times longer and >7 longer in the resistivity. The electronic transition appears to be a precursor to the structural transition.

We would like to acknowledge Dr. Jisun Kim and Dr. Kun Zhao for valuable discussion especially regarding experimental design and Dr. Kresimir Rupnik for providing equipment necessary to conduct the cooling process. We thank Dr. Yimei Zhu and Dr. Zhen Wang for valuable discussions.

References

[1] Coleman R V et al 1988 *Adv. Phys.* **37** 559
[2] Wilson J A, Di Salvo F J and Mahajan S 1975 *Adv. Phys.* **24** 117
[3] Yang J J et al 2012 *Phys. Rev. Lett.* **108** 116402
[4] Li B, Huang G, Sun J and Xing Z 2015 *Sci. Rep.* **4** 6433
[5] Pyon S, Kudo K and Nohara M 2012 *J. Phys. Soc. Jpn.* **81** 053701
[6] Ma Y et al 2015 *Phys. Rev.* B **92** 085427
[7] Manzeli S et al 2017 *Nat. Rev. Mater.* **2** 17033
[8] Choi W et al 2017 *Mater. Today* **20** 116
[9] Wang Q H et al 2012 *Nat. Nanotechnol.* **7** 699
[10] Cao H et al 2013 *Phys. Rev.* B **88** 115122
[11] Cao G et al 2017 *Phys. Rev.* B **95** 035148
[12] Pascut G L et al 2014 *Phys. Rev. Lett.* **112** 086402
[13] Peierls R E 1955 *Quantum Theory of Solids* (London: Oxford University Press)
[14] Ootsuki D et al 2012 *Phys. Rev.* B **86** 014519
[15] Fang A F et al 2013 *Sci. Rep.* **3** 1153
[16] Oh Y S, Yang J J, Horibe Y and Cheong S W 2013 *Phys. Rev. Lett.* **110** 127209
[17] Joseph B et al 2013 *Phys. Rev.* B **88** 224109
[18] Kim H S et al 2014 *Phys. Rev.* B **90** 201103(R)
[19] Eom M J et al 2014 *Phys. Rev. Lett.* **113** 266406
[20] Perdew J P, Burke K and Ernzerhof M 1996 *Phys. Rev. Lett.* **77** 3865
[21] Fradkin E et al 2010 *Annu. Rev. Condens. Matter Phys.* **1** 153
[22] Harter J W et al 2017 *Science* **356** 295
[23] Boyd R W 2008 *Nonlinear Optics* 3rd edn (San Diego: Academic Press)
[24] Shen Y R 1984 *The Principles of Nonlinear Optics* (New York: Wiley-Interscience)
[25] Hohlfeld J et al 2000 *Chem. Phys.* **251** 237
[26] Mizrahi V and Sipe J E 1988 *J. Opt. Soc. Am.* B **5** 660
[27] Hsieh D et al 2011 *Phys. Rev. Lett.* **106** 057401
[28] Mauerer T et al 2016 *Phys. Rev.* B **94** 014106
[29] Zhu Y and Wang Z 2018 Private communication
[30] Chen C et al 2017 *Phys. Rev.* B **95** 094118